



HAL
open science

Effect of the UV dose on the formation of complex organic molecules in astrophysical ices: irradiation of methanol ices at 20 K and 80 K

Laura I Tenelanda-Osorio, Alexis Bouquet, Thomas Javelle, Olivier Mousis, Fabrice Duvernay, Grégoire Danger

► **To cite this version:**

Laura I Tenelanda-Osorio, Alexis Bouquet, Thomas Javelle, Olivier Mousis, Fabrice Duvernay, et al.. Effect of the UV dose on the formation of complex organic molecules in astrophysical ices: irradiation of methanol ices at 20 K and 80 K. *Monthly Notices of the Royal Astronomical Society*, 2022, 515, pp.5009 - 5017. 10.1093/mnras/stac1932 . hal-03866166

HAL Id: hal-03866166

<https://hal.science/hal-03866166>

Submitted on 22 Nov 2022

HAL is a multi-disciplinary open access archive for the deposit and dissemination of scientific research documents, whether they are published or not. The documents may come from teaching and research institutions in France or abroad, or from public or private research centers.

L'archive ouverte pluridisciplinaire **HAL**, est destinée au dépôt et à la diffusion de documents scientifiques de niveau recherche, publiés ou non, émanant des établissements d'enseignement et de recherche français ou étrangers, des laboratoires publics ou privés.

Copyright

Effect of the UV dose on the formation of complex organic molecules in astrophysical ices: irradiation of methanol ices at 20 K and 80 K

Laura I. Tenelanda-Osorio,^{1,2} Alexis Bouquet,^{1,2} Thomas Javelle,¹ Olivier Mousis,² Fabrice Duvernay¹ and Grégoire Danger^{1,2,3}★

¹Aix–Marseille Université, CNRS, PIIM, Institut Origines, Marseille, F-13013, France

²Aix–Marseille Université, CNRS, CNES, LAM, Institut Origines, Marseille, F-13013, France

³Institut Universitaire de France, IUF, Paris, F-75005, France

Accepted 2022 July 5. Received 2022 July 5; in original form 2022 January 18

ABSTRACT

Methanol is a ubiquitous complex organic molecule (COM) in the interstellar medium, thought to be a precursor of larger COMs when it is submitted to different energetic processes, that can trigger chemical reactions in solid and gas phases. Using laboratory experiments, we report the characterization of the evolution of photoproducts generated by the UV irradiation of methanol ice at different UV doses and temperatures (20 and 80 K). We used gas chromatography coupled to mass spectrometry (GC-MS) to analyse the volatile organic compounds (VOCs) recovered during the warming of the photoprocessed methanol ice. We identified 21 molecules (with up to five carbon atoms, including alcohols, aldehydes, ketones, ester, and ethers) and followed their abundance as a function of the UV fluence and ice temperatures. With increasing UV fluence, an increase in the production of heavier COMs is observed, while species with 1 or 2 carbon atoms are depleted or do not increase. Species within a same chemical family show the same pattern of evolution, with heavier molecules present in smaller quantities. Ketones and esters are the chemical families that lead to more complex molecules and start forming at the earliest stages of irradiation. Their formation pathways are driven by radical recombinations with CO as the main building blocks. Aldehydes are formed before their alcohol counterparts, implying they do not form through alcohol dehydrogenation, but via radical recombination around HCO. Ethers seem to be the precursors of a large set of COMs, and alcohols present a steady profile throughout irradiation.

Key words: astrochemistry – molecular processes – ultraviolet: planetary systems.

1 INTRODUCTION

Ices have been detected in dense molecular clouds, protostars, and circumstellar discs (Van Dishoeck 2004; Boogert, Gerakines & Whittet 2015; Bergantini, Maksyutenko & Kaiser 2017; Rothard et al. 2017; Sie et al. 2019) and special attention has been paid to these ices due to the different energetic processes that they can undergo, including UV irradiation, electron bombardment, cosmic rays bombardment, and thermal chemistry, that allow solid state chemistry to occur in these objects (Nuevo et al. 2011; De Marcellus et al. 2015; Maity, Kaiser & Jones 2015; Paardekooper, Bossa & Linnartz 2016). In the early stages of stellar evolution, UV radiation can induce the photochemistry occurring in the protoplanetary disc. Newborn stars are a bright source of UV radiation (Gomez de Castro & Lamzin 2011), and cosmic rays that interact with hydrogen gas produce secondary UV photons that can reach the interior of the molecular cloud (Prasad & Tarafdar 1983; Cruz-Diaz et al. 2016; Sie et al. 2019). This radiation can alter the molecules in the ice, ionizing them or forming radicals that can later react to form more complex molecules (Mennella et al. 2001; Muñoz Caro et al. 2004; Martín-Doménech, Öberg & Rajappan 2020; Yocum et al. 2021). Solid-state reactions occurring in star-forming regions can lead to the formation

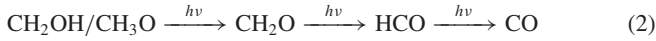
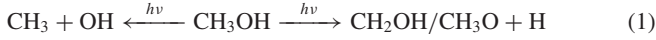
of Complex Organic Molecules (COMs) through mechanisms that otherwise cannot be explained by reactions in gas phase (Garrod, Weaver & Herbst 2008; Öberg et al. 2009; Linnartz et al. 2011; De Marcellus et al. 2015), since the lifetime of the molecules formed in gas phase is too short to allow the production of COMs (Gibb et al. 2004; Bennett & Kaiser 2007; Herbst 2014; Maity et al. 2015; Arumainayagam et al. 2019).

Laboratory studies on ice analogues are a tool to better understand the role of electromagnetic radiation in the formation of COMs (Gerakines, Moore & Hudson 2004), constrain chemical models of molecular clouds and star-forming regions (Bergantini et al. 2017; Arumainayagam et al. 2019), and determine the chemical pathways that led to several organic species observed in various astrophysical environments. Formation of COMs after warm-up of irradiated astrophysical ice analogues, together with observed relative abundance of COMs in molecular clouds, support the idea that COMs must be formed in the solid state on ice mantles and subsequently released to the gas phase (De Marcellus et al. 2015; Maity et al. 2015).

More than 200 molecules have been found throughout the interstellar medium (ISM), of which at least 60 have six atoms or more, including at least one carbon (Herbst & Van Dishoeck 2009; Herbst 2014; Maity et al. 2015; Muñoz Caro et al. 2019; Ciaravella et al. 2020). Several attempts have been made to determine the reaction pathways leading to those, by studying the products of the irradiation

* E-mail: gregoire.danger@univ-amu.fr

of ices and emulating their journey in the ISM, molecular clouds, and their arrival to planets, as they can also be pre-cometary and cometary material (Mumma et al. 2005; Bennett et al. 2007; De Marcellus et al. 2015). The simplest alcohol, methanol, is among these molecules. Due to its dissociation in CH_3 , OH , CH_3O , CH_2OH , and HCO radicals after irradiation (equations 1 and 2), it plays a role as precursor to form COMs after recombination of these radicals (Bernstein et al. 1995; Bennett et al. 2007; Öberg et al. 2009; De Barros et al. 2011; Paardekooper et al. 2016; Qasim et al. 2018; Yocum et al. 2021).



Methanol is found in protostellar molecular clouds, hot cores, and in interstellar ices, in both gas and solid phase, with an abundance varying between 5 and 30 percent relative to water; it is commonly used as an evolution indicator in star-forming regions (Jheeta et al. 2013; Herbst 2014; De Marcellus et al. 2015; Maity et al. 2015; Paardekooper et al. 2016; Butscher et al. 2017; Bergantini et al. 2018).

Laboratory experiments have been carried out involving irradiation of methanol with UV photons (Öberg et al. 2009; Henderson & Gudipati 2015; Abou Mrad et al. 2016; Paardekooper et al. 2016), X-ray photons (Chen et al. 2013a) and electrons (Bennett et al. 2007; Boamah et al. 2014; Maity et al. 2015), and its irradiation products have been analysed using laser desorption post-ionization time-of-flight mass spectrometry (LDPI TOF-MS) (Paardekooper et al. 2016), reflection-absorption infrared spectroscopy (RAIRS) with temperature programmed desorption (TPD) (Öberg et al. 2009), two-step laser ablation and ionization mass spectrometry (2S-LAIMS) (Henderson & Gudipati 2015), FT-IR (Bennett et al. 2007), TPD/QMS (Boamah et al. 2014), and gas chromatography coupled to mass spectrometry (GC-MS) (Abou Mrad et al. 2016). Common photoproducts after UV and electron irradiation include: CO_2 , formaldehyde (H_2CO), dimethyl ether (DME, CH_3OCH_3), acetaldehyde (CH_3CHO), methyl formate (HCOOCH_3), and ethanol ($\text{CH}_3\text{CH}_2\text{OH}$). These studies on methanol ice irradiation have focused on the identification of the molecular diversity formed after subjecting ice analogues to irradiation.

In this study, using Lyman- α VUV photons as radiation source, GC-MS as the main detection technique and FT-IR as a complementary diagnostic tool, we focus on the impact of the UV dose and temperature in the production rate of volatile organic compounds (VOCs) with up to five carbon atoms. This provides insights into the mechanisms at the origin of the detected COMs, on relationships between COM families, and possibly on astrophysical environments where molecular diversity production could be the highest.

2 METHODS

2.1 Experimental set-up

The experimental set-up consists of a stainless steel ultrahigh vacuum chamber. The chamber is operated at a base pressure of a few 10^{-8} mbar using a turbomolecular pump, and the sample holder is cooled down to 20 or 80 K using a closed cycle helium cryostat (modek 21 CTI). The tip of the cryostat holds the copper plated surface sample holder, which is suspended in the middle of the chamber and can be freely rotated to face deposition, irradiation, or IR-beam windows.

Pure methanol gas (for pesticide residue analysis, Fluka analytical from Sigma Aldrich) was pre-loaded into a glass-line at a pressure

of ~ 9 mbar, from which it was admitted into the vacuum chamber. The amount of methanol introduced in the chamber is controlled through the loss of methanol pressure in the glass-line: 0.2 mbar for experiments at 20 K, and 0.4 mbar for experiments at 80 K. Methanol does not condense on to the sample holder as readily at 80 K as it does at 20 K, resulting in the necessity to introduce a larger amount of methanol into the chamber to form a methanol layer of similar thickness, monitored by IR spectroscopy. The resulting ice was monitored using a Bruker Tensor 27 infrared spectrometer with a DTGS detector in reflection mode between 4000 and 600 cm^{-1} . Each spectrum was averaged over 20 scans with a 1 cm^{-1} resolution.

UV radiation was generated using a hydrogen-flow discharge lamp, continuously pumped while injecting hydrogen at a pressure typically within $430 - 470 \times 10^{-3}$ mbar, operated at 110 W and separated from the sample by a MgF_2 window. A comparable setup operated by Chen et al. (2013b) has been found to produce a flux of $\sim 6.4 \times 10^{13}$ photons $\text{cm}^{-2} \text{s}^{-1}$. We performed an evaluation of the photon flux using O_2 actinometry. To do so, we assume a distribution of photons similar to the one observed by Fulvio et al. (2014), who found the photon flux around 122 nm to be about 0.58 times the photon flux around 160 nm, and who used these results to re-evaluate the O_3 quantum yields of photons around these wavelengths.

We therefore calculate the photon flux using:

$$(\phi_{122} \times \text{QY}_{122} + \phi_{160} \times \text{QY}_{160}) \times t = \frac{\text{Area}(v_3)}{A(v_3)}, \quad (3)$$

where QY_{122} and QY_{160} are the O_3 quantum yields at 122 and 160 nm, respectively; ϕ_{122} and ϕ_{160} are the flux of photon around 122 and 160 nm, respectively (with $\phi_{122} = 0.58 \phi_{160}$, as discussed above), t is the time in s, $\text{Area}(v_3)$ is the area under the 1040 cm^{-1} absorption feature associated with O_3 , and $A(v_3)$ is the absorption strength of this feature (1.4×10^{-17} cm per molecule; Teolis, Famá & Baragiola 2007). We obtain a total photon flux ($\phi_{122} + \phi_{160}$) of about $1\text{E}13$ photons $\text{s}^{-1} \text{cm}^{-2}$ at the target. We emphasize that due to the inability to verify our assumptions on the shape of the UV emission spectrum, as well as the error margins on the UV flux (and therefore O_3 quantum yield) obtained by Fulvio et al., this result should be taken as an order of magnitude. Different irradiation times were tested: 0.25, 0.5, 1, 3, 8, and 24 h (corresponding to 9×10^{15} , 1.8×10^{16} , 3.6×10^{16} , 1.08×10^{17} , 2.88×10^{17} , and 8.64×10^{17} photons cm^{-2} , respectively).

At 20 K, 0.25, 0.5, and 1 h were performed three times, and 3, 8, and 24 h were performed twice. At 80 K, 1, 3, and 24 h were performed twice and 0.5 h was performed once.

Each experiment consisted in the deposition of a layer of methanol about 0.1 μm thick ($\sim 1.2 \times 10^{17}$ molecules cm^{-2} , based on the amorphous methanol band strength and density obtained by Luna et al. 2018 at 20 K) and its subsequent irradiation. After irradiation, the loss of methanol was quantified by FT-IR spectroscopy, using the methanol band at 1026 cm^{-1} . To increase the quantity of products for GC-MS analysis, five irradiated layers were formed in each experiment, by depositing and irradiating a new layer on top of the previous (irradiated) one. Subsequently the sample was brought back to room temperature and the volatiles thus released in gas phase and transferred to a pre-concentration loop using the VAHIAA setup (described in Abou Mrad et al. 2014), to be injected into the GC-MS using helium as a carrier gas at a constant flow rate of 1.18 mL min^{-1} . The GC-MS is a Thermofisher, GC Trace 1310 and MS ion trap ITQ 900, modified in collaboration with Interscience Belgium for gaseous sample injection. Samples were transferred to the GC split/splitless injector with a split ratio of 10 at 250°C. The error introduced by the injection towards the GC-MS was also determined. This was done by

introducing a known amount of methanol into the pre-concentration loop and transferring it into the GC–MS in the same way as any of our samples. The variation of methanol quantity over multiple repetitions of this process was found to be within 11 per cent of the average.

VOCs were separated on an Rxi®–624 Sil MS (60 m × 0.25 mm i.d. × 1.4 μm d.f.) capillary column purchased from Restek. Initial column temperature was set at 40°C for 3 min, followed by an increase of 5°C min⁻¹ to 150°C, then of 20°C min⁻¹ until 220°C.

The mass spectrometer transfer line was set to 250°C. The ion source temperature was set to 250°C and the maximum ion time in the trap was 25 ms. The ion trap mass spectrometer was used in the electron impact ionization mode with an ionization energy of 70 eV. The signal was collected with a full scan mode in the mass range between 15 and 300 u.

We verified that the thickness of a typical layer was sufficient to prevent unwanted over-irradiation (i.e. that when irradiating layer $n + 1$, layer n is unaffected) by performing experiments using ¹³CH₃OH and CO₂. They consisted in depositing a layer of ¹³CH₃OH (0.1, 0.2, or 0.3 mbar) on top of a layer of 0.1 mbar of CO₂, irradiating the top layer during 24 h and checking for formation of ¹²CO (using the 2138 cm⁻¹ band). After this time the formation of ¹²CO was negligible.

In order to discard contamination of the system or the methanol, and other processes, three blank experiments were run. Each consisted of the deposition of five layers of methanol on the sample holder, followed by transfer to the GC–MS with the same conditions and procedure but without any irradiation.

2.2 Data analysis

The chromatographic peaks of the VOCs recovered were compared with a data base including 69 standards (see supplementary information). The retention time and mass spectra of the standards were obtained using the same procedure as the irradiated samples by Abou Mrad et al. (2014), who individually or in mixtures, introduced the 69 standards (including alcohols, aldehydes, ketones, acids, esters, and ethers with up to 6 atoms) directly into the VAHIA set-up, based on the expected photoproducts of methanol irradiation, using the same procedure as the irradiated sample. 3.5 μmol of each standard were introduced.

The identification is considered as relevant if the VOC retention time falls within 95 per cent of confidence interval of the standard and the fragmentation pattern is in accordance with the standard's. Details are given in Abou Mrad et al. (2014). In the case of CO₂, dimethyl ether and 2-butanone, these were identified using their mass spectra reported in the NIST Chemistry WebBook (<https://webbook.nist.gov/chemistry/>). For each compound identified we measured the absolute area under the total ion current curve (TIC) of the chromatogram, which is a function of the abundance of the compound, and estimated the number of molecules for each experiments in mol, based on the sensitivity coefficients deduced from the standards.

Integrated TICs of blank were subtracted to integrated TICs obtained in each experiments.

3 RESULTS

3.1 Effect of UV dose on methanol ice at 20 K

The irradiation of methanol ice led to the formation of at least 21 VOCs (Fig. 1), identified in Table 1. After 15 min of irradiation (Fig. 2), 12 molecules are already detected, ranging from C1 (with

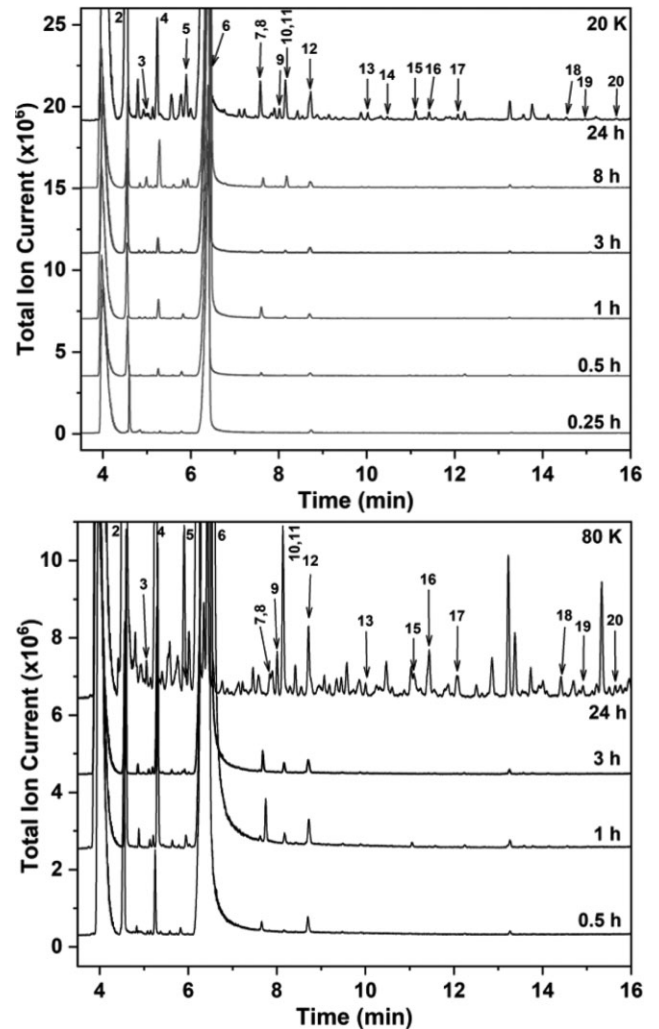


Figure 1. Top: chromatograms of VOCs formed at 20 K. Bottom: chromatograms of VOCs formed at 80 K.

one carbon atom) to more complex C5 (with five carbon atoms). These include: CO and CO₂ (C1, not in the figure); two ethers: DME (C2) and diethylether (C4); three ketones: acetone (C3), butanone (C4) and 2-propanone (C5); one aldehyde: isobutyraldehyde (C4) (tentative identification); and four esters: methyl formate (C2), methyl acetate (C3), methyl propionate (C4), and methyl butyrate (C5). After 3 h, all final compounds appear (Table 1).

Most of the identified VOCs are aldehydes (5 species), followed by esters (4 species). Esters and ketones are the chemical families with the heaviest molecules, up to C5. Aside from these exceptions, this observation is consistent with the radical chemistry that occurs during the photoprocessing, where molecules with higher complexity decrease in abundance due to the decrease in the probability of radicals to encounter (Bockelée-Morvan et al. 2004; Pizzarello, Cooper & Flynn 2006; Garrod et al. 2008; Herbst & Van Dishoeck 2009; Bossa et al. 2015; Abou Mrad et al. 2016; Öberg 2016). C1/C2 compounds are up to two order of magnitude more abundant than C5 (up to 10⁻⁶ mol versus ~10⁻⁸ mol at most).

Furthermore, Fig. 3 shows that each family seems to have its own pattern of evolution. Impressively, the molecular diversity of esters appears at low dose, after 15 min of irradiation, when C2 to C5 esters are already present. We identified methyl formate (HCOOCH₃), methyl acetate (CH₃COOCH₃), methyl propionate

Table 1. Compounds identified by GC-MS analysis after methanol ice irradiation at 20 K and subsequent warm up to 300 K. R_t : retention time, m/z: mass-to-charge ratio of the main ions used for identification.

No.	Species	R_t sample	R_t standard (min)	m/z	Molecular structure
	Carbon monoxide (CO)	3.98	–	28 12 16 *	<chem>C=O</chem>
2	Carbon dioxide (CO ₂)	4.54	4.34	44 28 16	<chem>O=C=O</chem>
3	Formaldehyde (H ₂ CO)	4.96	4.77	29 28 30	<chem>H2C=O</chem>
4	Dimethyl ether (CH ₃ OCH ₃)	5.25	–	45 46 29 *	<chem>COC</chem>
5	Acetaldehyde (CH ₃ CHO)	5.91	5.74	43 29 44	<chem>CC=O</chem>
6	Methyl formate (HCOOCH ₃)	6.43	6.31	31 60 61	<chem>COC=O</chem>
7	Diethyl ether (CH ₃ CH ₂ OCH ₂ CH ₃)	7.61	7.61	31 59 41	<chem>CCOCC</chem>
8	Ethanol (CH ₃ CH ₂ OH)	7.62	7.26	45 31 29	<chem>CCO</chem>
9	Propionaldehyde (CH ₃ CH ₂ CHO)	8.03	8.05	57 29 27	<chem>CCC=O</chem>
10	Acetone ((CH ₃) ₂ CO)	8.14	8.15	43 58 42	<chem>CC(=O)C</chem>
11	Dimethoxymethane (CH ₃ OCH ₂ OCH ₃)	8.16	8.21	75 45 29	<chem>COCOC</chem>
12	Methyl acetate (CH ₃ COOCH ₃)	8.72	8.81	43 74 42	<chem>COC(=O)C</chem>
13	Isobutyraldehyde ((CH ₃) ₂ CHCHO) (tentative)	10.05	10.06	41 43 39	<chem>CC(C)C=O</chem>
14	Propanol (CH ₃ CH ₂ CH ₂ OH)	10.49	10.52	31 41 39	<chem>CCCO</chem>
15	Butyraldehyde (CH ₃ CH ₂ CH ₂ CHO)	11.13	11.36	43 41 44	<chem>CCCC=O</chem>
16	2-Butanone (CH ₃ COCH ₂ CH ₃)	11.36	–	43 72 29 *	<chem>CCC(=O)C</chem>
17	Methyl propionate (CH ₃ CH ₂ CO ₂ CH ₃)	12.08	12.38	57 29 88	<chem>COC(=O)CC</chem>
18	Butanol (CH ₃ CH ₂ CH ₂ CH ₂ OH)	14.56	14.61	56 31 41	<chem>CCCCO</chem>
19	2-Pentanone (CH ₃ COCH ₂ CH ₂ CH ₃)	15.00	15.32	43 86 71	<chem>CCC(=O)CC</chem>
20	Methyl butyrate (CH ₃ CH ₂ CH ₂ CO ₂ CH ₃)	15.70	16.09	43 103 74	<chem>COC(=O)CCC</chem>

Note. *m/z reported at NIST.

(CH₃CH₂CO₂CH₃), and methyl butyrate (CH₃CH₂CH₂CO₂CH₃). Their production rate seems to increase constantly over time. Ketones also display a non-negligible molecular diversity after 15 min. We identified: acetone ((CH₃)₂CO), butanone (CH₃COCH₂CH₃), and 2-pentanone (CH₃COCH₂CH₂CH₃). Butanone is the main C4 product with a final quantity higher than 10⁻⁸ mol, and 2-pentanone is the main C5 product with a final quantity close to 10⁻⁸ mol.

Aldehydes, formaldehyde (CH₂O), propionaldehyde (C₂H₆O), butyraldehyde (C₄H₈O), were identified and possibly isobutyraldehyde (C₄H₈O). They appear after 1 h of irradiation. Interestingly, C1 and C2 appear after C3 to C5 compounds. After 8 h of irradiation, the quantity of the heaviest aldehydes (C4) keeps increasing, although with a lower rate, while the quantity of CH₂O is lower, which means either the production rate decreases or it is being consumed to form

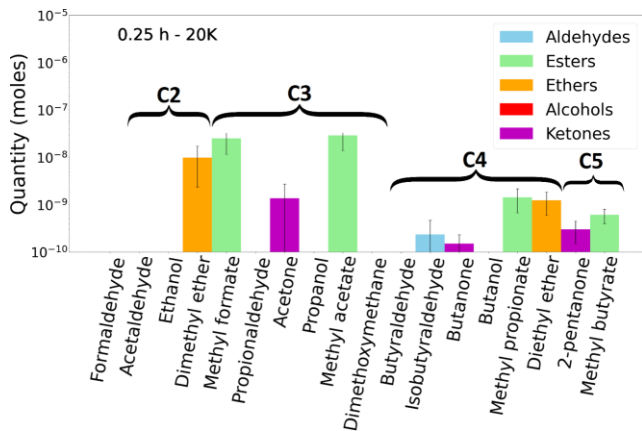


Figure 2. VOCs formed after 15 min of irradiation at 20 K.

other molecules. It however reaches the highest abundance among all the identified molecules.

Ethers, DME, and diethyl ether are formed rapidly after 15 min of irradiation. During the first hour the production of DME tends to increase. After, the measured quantity fluctuates around 10^{-6} mol. Diethyl ether increases as DME during the first hour where it reaches its highest abundance and then decreases to a steady state around 10^{-9} mol at 3 h. Dimethoxymethane appears after 30 min of irradiation and increases up to 8 h and then it fluctuates with a similar rate to DME.

Alcohols are the chemical family that form the latest, being the only one of which no species were detected after 15 min of irradiation (besides methanol). Ethanol is detectable only after 30 min of irradiation, while propanol and butanol are observable only after 3 and 1 h of irradiation, respectively. All alcohols reach a steady state after 8 h of irradiation.

These observations demonstrate that chemical pathways leading to the species observed strongly depend on the chemical families.

3.2 Effect of temperature

As observed at 20 K, the formation of photoproducts at 80 K also tends to decrease with the increase of carbon atoms in the molecules (Fig. 4). Furthermore, a specific pattern by chemical families is observed at early irradiation time. After 24 h of irradiation at 80 K, except for propanol that does not appear, the VOCs formed are the same than those observed at 20 K. Aldehydes are formed after 3 h of irradiation at 80 K, except for the possible isobutyraldehyde which is found in all experiments with a quantity of the same order than at 20 K. The same ketones appear at 80 K than at 20 K, exhibiting the same pattern, with increasing quantity proportionally with time. Butanone and 2-pentanone are the main C4 and C5 products, respectively. Ethanol and butanol appear at all times at 80 K, while at 20 K butanol is not detected after 30 min of irradiation. DME is detected from 1 h of irradiation at 80 K, at a larger quantity than at 20 K. Diethyl ether and dimethoxymethane appear from 30 min.

At 80 K, a higher dose is required to form the products observed at 20 K. As shown in Fig. 5, after 30 min of irradiation at 20 K, 14 VOCs are already formed while at 80 K only 11 are formed, of which butanol does not appear at 20 K whereas butyraldehyde is observed. These observations suggest that production yields of compounds are different at 80 K compared to 20 K.

4 DISCUSSION

4.1 Implication for COMs formation

Our results have to be compared with previous works such as electron irradiation experiments (Bennett et al. 2007). When solid methanol is irradiated with electrons (5.9×10^{14} electrons cm^{-2}) (Bennett et al. 2007), the formation of formaldehyde is observed at the very beginning (before one hour) of the irradiation. This is not the case in our experiments: formaldehyde is only detected after one hour of irradiation ($\sim 3.6 \times 10^{18}$ photons cm^{-2}) at 20 K. There is instead a high production of DME and methyl acetate, which seem to be favoured during the first stages of irradiation.

In comparison, ethanol, which is a DME isomer, is formed at higher UV dose, appearing after 30 min of irradiation.

This difference in behaviour between the two isomers may find its origin in the quantity of radicals formed during the photolysis of methanol. DME may form from the radical–radical recombination of CH_3 and OCH_3 radicals (equation 4) while its isomer, ethanol can be formed from the radical–radical recombination of CH_3 and CH_2OH (equation 5). This suggest that OCH_3 radicals are formed in larger quantity than CH_2OH radicals. These results totally agree with the recent works done by Yocum et al. (2021) and Gutiérrez-Quintanilla et al. (2021).



In addition, the methylformate detection at the early stage of irradiation is also consistent with the OCH_3 radicals being one of the most abundant radicals formed from methanol photolysis. Indeed methylformate is supposed to be formed from $\text{HCO} + \text{OCH}_3$ radical–radical recombination (equation 6) (Bennett et al. 2007; Bennett & Kaiser 2007; Öberg et al. 2009; Gutiérrez-Quintanilla et al. 2021).



Although the results in this study concerning the branching ratio between OCH_3 and CH_2OH seem to support experimental works (Gutiérrez-Quintanilla et al. 2021; Yocum et al. 2021) and theoretical claims (Laas et al. 2011), this is in contradiction with previous experimental work done by Öberg et al. (2009) which determine a branching ratio $\text{CH}_2\text{OH}:\text{OCH}_3$ 5:<1. This discrepancies could come from the technique used for product identification and quantification. In Öberg et al. (2009), the product quantification is made from IR spectra in the solid phase while in Yocum et al. (2021) – as well as in this study – the product identification is made in the gas phase with more accurate techniques for characterization and quantification, namely submillimetre/far-IR spectroscopy and GC-MS, respectively. Furthermore, if diethylether formation follows the same sort of radical recombination, i.e. between $\text{CH}_3\text{CH}_2\text{O}$ and CH_2CH_3 (equation 7), this could also explain the late ethanol appearance, with diethylether and ethanol formation in competition.



Once formed, ethanol, by its dehydrogenation (equation 8), could be a precursor of acetaldehyde, the latter being formed at higher UV doses (1 h versus 30 min for ethanol). This is corroborated by the work of Gutiérrez-Quintanilla et al. (2021) who did not observe acetaldehyde formation when methanol was isolated in argon matrix, a technique that provides the recombination of the first generation radical (CH_3 , CH_3O , CH_2OH , OH , HCO) without any photodegradation of recombination products (ethanol to acetaldehyde for instance).

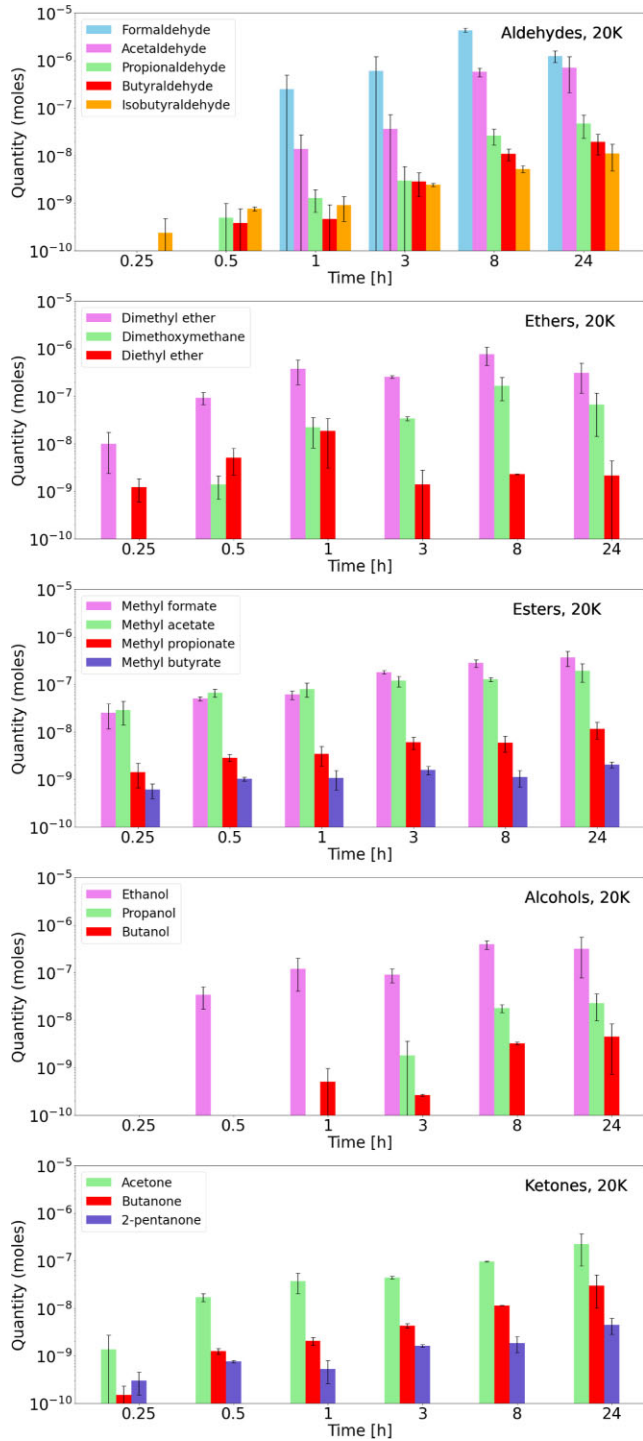


Figure 3. Evolution of VOCs quantity identified at 20 K by families.

Another mechanism to form acetaldehyde could be a recombination between HCO and CH₃ radicals (equation 9). However, a theoretical study showed that this recombination does not favour acetaldehyde formation but the H abstraction leading to CH₄ and CO formation (equation 10) (Enrique-Romero et al. 2021).

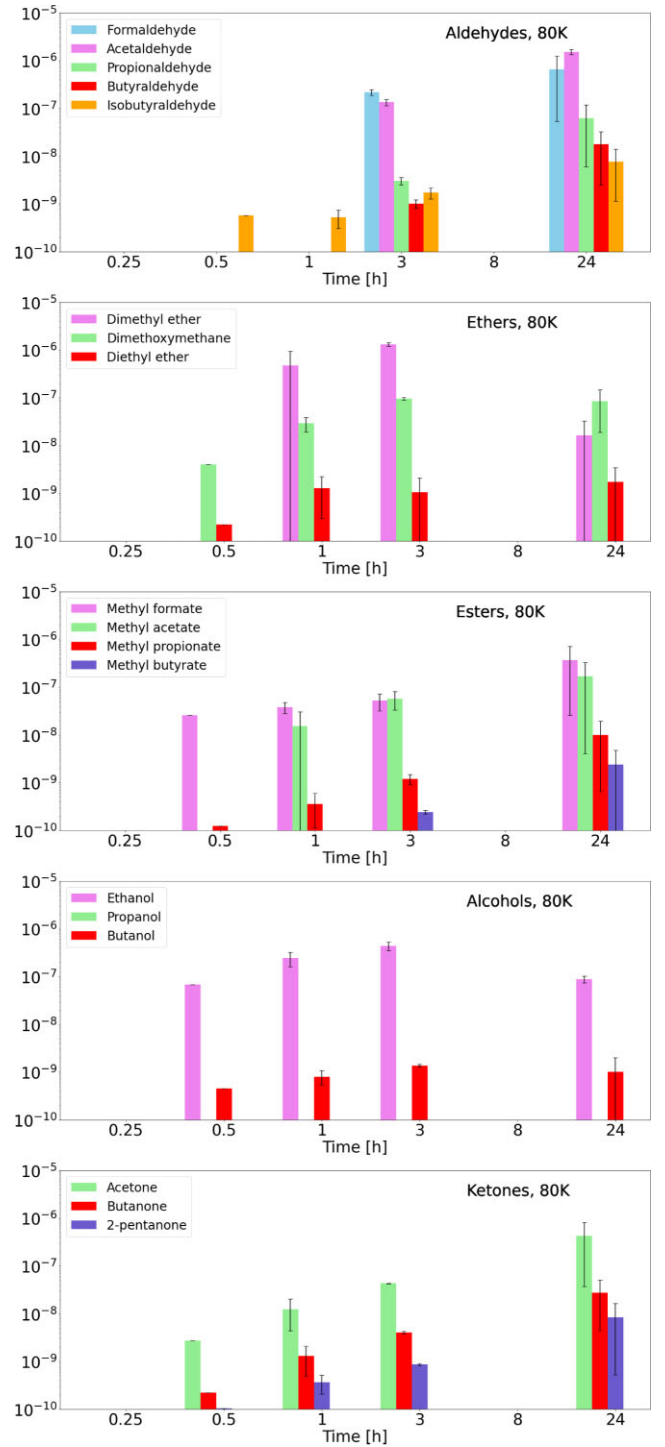


Figure 4. Evolution of VOCs quantity identified at 80 K by families. No 0.25 h or 8 h experiments were performed at this temperature.



Nevertheless, this cannot be generalized, since other aldehydes are formed before their potential alcohol precursors. Furthermore, heavier aldehydes are detected at lower UV doses than acetaldehyde, excluding a possible formation by elongation of the alkyl chain of acetaldehyde. For aldehydes other than acetaldehyde, a recombination between HCO and the radical of alkyl chain can be considered

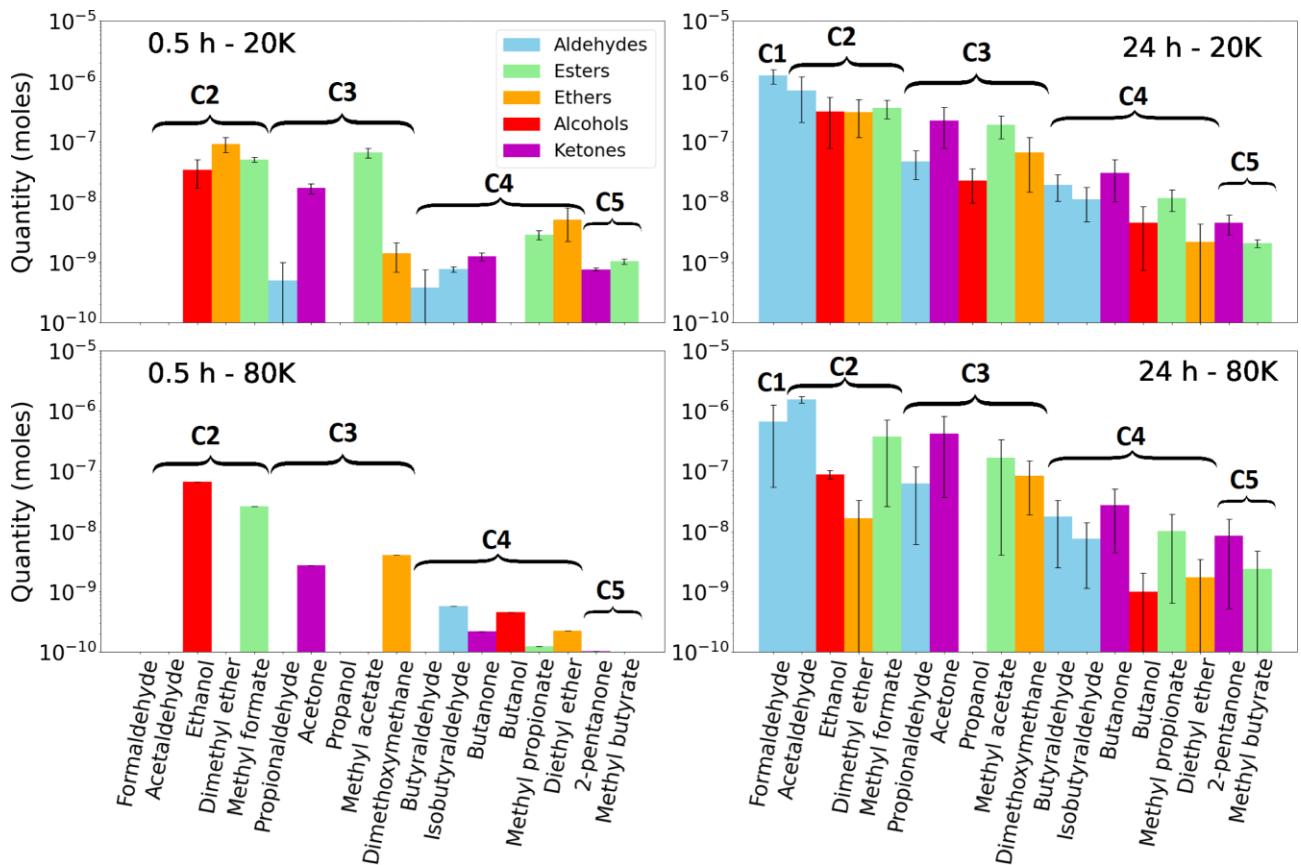
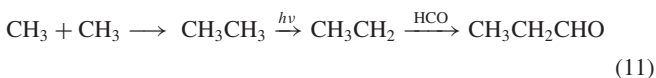


Figure 5. Quantity (mol) of the VOCs formed at 20 and 80 K after 30 min and 24 h of UV irradiation.

(equation 11, i.e. propionaldehyde). This would be coherent with Abou Mrad et al. (2017) who observed an increase of aldehydes once water was added to a methanol ice, increasing the HCO yield, suggesting a formation from radical recombination with HCO rather than from alcohol dehydrogenation.

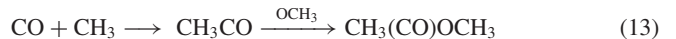


Conversely, hydrogenation of aldehydes could be a source of alcohols. For instance, propanol could be formed via hydrogenation of propionaldehyde (equation 12), which initially forms via radical-radical reactions equation (11) (Qasim et al. 2019).



Interestingly, for certain chemical families, formation of heavier and more complex molecules at very low UV dose are observed, mainly for esters and ketones (C2 to C5 at 15 min of irradiation). All esters detected in this work are methyl esters. This could be related to the high production of OCH_3 radical as observed for DME. Ester formation seems to be uncorrelated with aldehydes, since aldehydes appear at higher UV doses, but correlated to ketones, as they follow a similar trend, formed at early irradiation (15 min). The key intermediate for their formation could be CO that is formed from methanol irradiation and observed at low UV doses with FT-IR. Esters could then be formed by the radical recombination between alkane radical, CO and OCH_3 . For instance, methyl acetate could be formed from CH_3 , CO, and OCH_3 (equation 13). This is consistent

with the fast formation of DME and diethylether.



A similar mechanism could be expected for ketones, which follow the same trend than esters. Even if reactions of radicals with CO require energy which could be unavailable at low temperature (20 K), this mechanism is supported by the detection of CO_2 in our experiments. CO_2 is indeed formed by the reaction between CO and OH that occurs at low temperature (Ioppolo et al. 2011; Noble et al. 2011; Zins, Joshi & Krim 2011; Arasa et al. 2013; Gutiérrez-Quintanilla et al. 2021), implying that at 20 K a sufficient amount of energy is available.

COMs observed at 20 K are observed at higher UV doses at 80 K. Furthermore, they present lower abundances at 80 K for a same UV dose. Since the COMs observed are mainly formed through radical recombinations, higher temperatures could interfere in these mechanisms. At higher temperatures the sublimation rate of lighter COMs increases and radical migrations in the methanol matrix are probably faster, implying a higher desorption rate as well as higher rates of neutralization of first generation radicals (CH_3 , $\text{CH}_3\text{O}\dots$). This would decrease precursor abundances and thus a higher UV doses would be needed to reach a sufficient abundance of precursors, allowing the formation and detection of the COMs observed at 20 K.

4.2 Astrophysical implications

All the C1 and C2 species detected in this study have been observed in previous studies using VUV as radiation source (Öberg et al. 2009;

Maity et al. 2015; Paardekooper et al. 2016) and they have all been observed in the ISM. Results reported here support COMs formation on interstellar grains from radical–radical recombinations. However, it does not mean that iCOMs are exclusively formed on grains but that probably other routes coexist such as gas phase formation. The relative contribution of gas phase versus grain formation may depend on physical conditions (temperature, density, UV flux, etc.).

The difference in the evolution of quantity produced over time at different temperatures can give insight on the different products that can be found in different protoplanetary discs. These experimental conditions can be compared with those derived from the model developed by Ciesla & Sandford (2012), which describes the exposure of ice grains to the UV flux during their dynamical evolution within the protosolar nebula (PSN). In their nominal model, Ciesla & Sandford (2012) find that a typical dosage for particles with 1 micron radii is about 5×10^{12} photons after 1 Myr of radial and vertical transport within the disc, and assuming a nominal interstellar UV flux of 10^8 photons $\text{cm}^{-2} \text{s}^{-1}$ (Habing 1968). The comparison of this dose (1.59×10^{20} photons cm^{-2}) with the aforementioned value (9×10^{17} photons cm^{-2}) suggests that only ~ 5.6 kyr of UV irradiation within the disc is enough to provide an identical value. This extremely short time-scale suggests that methanol included in micron-sized grains can be efficiently converted into COMs well before they grow and form larger solids in the protosolar nebula.

In addition, the temperatures of 20 K and 80 K adopted in our experiments correspond to the ~ 30 and 10 AU regions of the disc mid-plane, respectively, assuming its characteristics are similar to those of the PSN (Mousis et al. 2020). This outer region of the disc brackets the formation zone of the building blocks of the giant planets, satellites, and comets in the PSN, implying that COMs may have contributed to the composition of these solids.

5 CONCLUSIONS

Methanol ices subjected to UV irradiation led to the formation of COMs including aldehydes, ketones, esters, ethers, and heavier alcohols. For some families such as esters and ketones, complex molecules with up to five carbon atoms are formed at low UV dose (9.00×10^{17} photons cm^{-2}). At low temperatures (20 K), the pattern of quantity produced along different periods of time seems to be similar according to the functional group. Most of the identified VOCs are formed from the recombination of methanol radicals, and CO seems to be an important intermediate, principally for esters and ketones. Conversely, alcohols seem to form from the hydrogenation of aldehydes. Increasing the temperature of irradiation (80 K) affects the fluence at which compounds start to form. Most of the VOCs seen early at 20 K, appear at 80 K only after 3 h of irradiation. Even though the products at 20 K and 80 K are the same (except for propanol), their different abundance through different times of irradiation might support different pathways in different environments such as cool or warm planetary discs.

ACKNOWLEDGEMENTS

The research was funded with support from the Centre National d'Etudes Spatiales (CNES, R-S18/SU-0003-072 and R-S18/SU-0003-072, PI: GD), and the French Centre National de la Recherche Scientifique (CNRS) with the programs 'Physique et Chimie du Milieu Interstellaire' (PCMI- PI: GD) and 'Programme National de Planétologie' (PNP) (GD, AB). GD is grateful to the Agence nationale de la recherche for funding via ANRs RAHIIA-SSOM (ANR-16-CE29-0015) and VAHIIA (ANR-12-JS08-0001).

DATA AVAILABILITY STATEMENT

The data underlying this article will be shared on reasonable request to the corresponding author.

REFERENCES

- Abou Mrad N., Duvernay F., Theulé P., Chiavassa T., Danger G., 2014, *Anal. Chem.*, 86, 8391
- Abou Mrad N., Duvernay F., Chiavassa T., Danger G., 2016, *MNRAS*, 458, 1234
- Abou Mrad N., Duvernay F., Isnard R., Chiavassa T., Danger G., 2017, *ApJ*, 846, 124
- Arasa C., van Hemert M. C., van Dishoeck E. F., Kroes G.-J., 2013, *J. Phys. Chem. A*, 117, 7064
- Arumainayagam C. R. et al., 2019, *Chem. Soc. Rev.*, 48, 2293
- Bennett C. J., Kaiser R. I., 2007, *ApJ*, 661, 899
- Bennett C. J., Chen S.-H., Sun B.-J., Chang A. H., Kaiser R. I., 2007, *ApJ*, 660, 1588
- Bergantini A., Maksyutenko P., Kaiser R. I., 2017, *ApJ*, 841, 96
- Bergantini A., Góbi S., Abplanalp M. J., Kaiser R. I., 2018, *ApJ*, 852, 70
- Bernstein M. P., Sandford S. A., Allamandola L. J., Chang S., Scharberg M. A., 1995, *ApJ*, 454, 327
- Boamah M. D. et al., 2014, *Faraday Discuss.*, 168, 249
- Bockelée-Morvan D., Crovisier J., Mumma M., Weaver H., 2004, *Comets II*, 1, 391
- Boogert A. A., Gerakines P. A., Whittet D. C., 2015, *ARA&A*, 53, 541
- Bossa J.-B., Paardekooper D., Isokoski K., Linnartz H., 2015, *Phys. Chem. Chem. Phys.*, 17, 17346
- Butscher T., Duvernay F., Rimola A., Segado-Centellas M., Chiavassa T., 2017, *Phys. Chem. Chem. Phys.*, 19, 2857
- Chen Y.-J., Ciaravella A., Muñoz Caro G. M., Cecchi-Pestellini C., Jiménez-Escobar A., Juang K.-J., Yih T.-S., 2013a, *ApJ*, 778, 162
- Chen Y.-J., Chuang K.-J., Muñoz Caro G. M., Nuevo M., Chu C.-C., Yih T.-S., Ip W.-H., Wu C.-Y., 2013b, *ApJ*, 781, 15
- Ciaravella A., Muñoz Caro G. M., Jiménez-Escobar A., Cecchi-Pestellini C., Hsiao L.-C., Huang C.-H., Chen Y.-J., 2020, *Proc. Natl Acad. Sci.*, 117, 16149
- Ciesla F. J., Sandford S. A., 2012, *Science*, 336, 452
- Cruz-Díaz G. A., Martín-Doménech R., Muñoz Caro G. M., Chen Y.-J., 2016, *A&A*, 592, A68
- De Barros A., Domaracka A., Andrade D., Boduch P., Rothard H., Da Silveira E., 2011, *MNRAS*, 418, 1363
- De Marcellus P., Meinert C., Myrgorodska I., Nahon L., Buhse T., d'Hendecourt L. L. S., Meierhenrich U. J., 2015, *Proc. Natl Acad. Sci.*, 112, 965
- Enrique-Romero J., Ceccarelli C., Rimola A., Skouteris D., Balucani N., Ugliengo P., 2021, *A&A*, 655, A9
- Fulvio D., Brieva A., Cuyllé S., Linnartz H., Jäger C., Henning T., 2014, *Appl. Phys. Lett.*, 105, 014105
- Garrod R. T., Weaver S. L. W., Herbst E., 2008, *ApJ*, 682, 283
- Gerakines P., Moore M., Hudson R., 2004, *Icarus*, 170, 202
- Gibb E., Whittet D., Boogert A., Tielens A., 2004, *ApJS*, 151, 35
- Gomez de Castro A. I., Lamzin S. A., 2011, *Astrophys. Space Sci.*, 335, 61
- Gutiérrez-Quintanilla A. et al., 2021, *MNRAS*, 506, 3734
- Habing H. J., 1968, *Bull. Astron. Inst. Netherlands*, 19, 421
- Henderson B. L., Gudipati M. S., 2015, *ApJ*, 800, 66
- Herbst E., 2014, *Phys. Chem. Chem. Phys.*, 16, 3344
- Herbst E., Van Dishoeck E. F., 2009, *ARA&A*, 47, 427
- Ioppolo S., Van Boheemen Y., Cuppen H., Van Dishoeck E., Linnartz H., 2011, *MNRAS*, 413, 2281
- Jheeta S., Domaracka A., Ptasińska S., Sivaraman B., Mason N., 2013, *Chem. Phys. Lett.*, 556, 359
- Laas J. C., Garrod R. T., Herbst E., Weaver S. L. W., 2011, *ApJ*, 728, 71
- Linnartz H. et al., 2011, in *Proc. IAU Symp. 7, Solid State Pathways towards Molecular Complexity in Space*. Cambridge Univ. Press, Cambridge, p. 390

Luna R., Molpeceres G., Ortigoso J., Satorre M. A., Domingo M., Maté B., 2018, *A&A*, 617, A116

Maity S., Kaiser R. I., Jones B. M., 2015, *Phys. Chem. Chem. Phys.*, 17, 3081

Martín-Doménech R., Öberg K. I., Rajappan M., 2020, *ApJ*, 894, 98

Mennella V., Caro G. M. M., Ruitkamp R., Schutte W., Greenberg J., Brucato J., Colangeli L., 2001, *A&A*, 367, 355

Mousis O., Aguichine A., Helled R., Irwin P. G. J., Lunine J. I., 2020, *Philos. Trans. R. Soc. A*, 378, 20200107

Mumma M. J. et al., 2005, *Science*, 310, 270

Muñoz Caro G. M., Ciaravella A., Jiménez-Escobar A., Cecchi-Pestellini C., González-Díaz C., Chen Y.-J., 2019, *ACS Earth Space Chem.*, 3, 2138

Muñoz Caro G. M., Meierhenrich U., Schutte W., Greenberg J., 2004, *A&A*, 413, 209

Noble J. A., Dulieu F., Congiu E., Fraser H. J., 2011, *ApJ*, 735, 121

Nuevo M., Milam S., Sandford S., De Gregorio B., Cody G., Kilcoyne A., 2011, *Adv. Space Res.*, 48, 1126

Öberg K. I., 2016, *Chem. Rev.*, 116, 9631

Öberg K. I., Garrod R. T., Van Dishoeck E. F., Linnartz H., 2009, *A&A*, 504, 891

Paardekooper D., Bossa J.-B., Linnartz H., 2016, *A&A*, 592, A67

Pizzarello S., Cooper G., Flynn G., 2006, in Lauretta D. S., McSween H. Y., eds, *Meteorites and the early Solar system II*, Vol. 1. University of Arizona Press, Tucson, p. 625

Prasad S. S., Tarafdar S. P., 1983, *ApJ*, 267, 603

Qasim D., Chuang K.-J., Fedoseev G., Ioppolo S., Boogert A., Linnartz H., 2018, *A&A*, 612, A83

Qasim D. et al., 2019, *A&A*, 627, A1

Rothard H., Domaracka A., Boduch P., Palumbo M. E., Strazzulla G., Da Silveira E. F., Dartois E., 2017, *J. Phys. B: At. Mol. Opt. Phys.*, 50, 062001

Sie N.-E., Muñoz Caro G. M., Huang Z.-H., Martín-Doménech R., Fuente A., Chen Y.-J., 2019, *ApJ*, 874, 35

Teolis B., Famá M., Baragiola R., 2007, *J. Chem. Phys.*, 127, 074507

Van Dishoeck E. F., 2004, *ARA&A*, 42, 119

Yocum K., Milam S., Gerakines P., Weaver S. W., 2021, *ApJ*, 913, 61

Zins E.-L., Joshi P. R., Krim L., 2011, *ApJ*, 738, 175

SUPPORTING INFORMATION

Supplementary data are available at [MNRAS](https://www.mnras.org) online.

Table S1. Standard compounds. Detected compounds are highlighted in bold.

Figure S1. Comparison of mass spectra acquired in the 20 K and 80 K experiments with the standard of the proposed identification (Formaldehyde, acetaldehyde, ethanol).

Figure S2. Comparison of mass spectra acquired in the 20 K and 80 K experiments with the standard of the proposed identification (Dimethyl ether, methylformate, propionaldehyde).

Figure S3. Comparison of mass spectra acquired in the 20 K and 80 K experiments with the standard of the proposed identification (Acetone, dimethoxymethane, propanol).

Figure S4. Comparison of mass spectra acquired in the 20 K and 80 K experiments with the standard of the proposed identification (Methyl acetate, possible isobutyraldehyde, 2-butanone).

Figure S5. Comparison of mass spectra acquired in the 20 K and 80 K experiments with the standard of the proposed identification (Butanol, Methyl propionate, 2-pentanone).

Figure S6. Comparison of mass spectra acquired in the 20 K and 80 K experiments with the standard of the proposed identification (Methyl butyrate).

Please note: Oxford University Press is not responsible for the content or functionality of any supporting materials supplied by the authors. Any queries (other than missing material) should be directed to the corresponding author for the article.

This paper has been typeset from a $\text{\TeX}/\text{\LaTeX}$ file prepared by the author.